THE JOURNAL OF PHYSICAL CHEMISTRY B

Article

pubs.acs.org/JPCB

MD and QM/MM Studies on Long-Chain L-α-Hydroxy Acid Oxidase: Substrate Binding Features and Oxidation Mechanism

Yang Cao, Shuang Han, Lushan Yu, Haiyan Qian, and Jian-Zhong Chen*

Institute of Materia Medica, College of Pharmaceutical Sciences, Zijingang Campus, Zhejiang University, 866 Yuhangtang Rd., Hangzhou, Zhejiang 310058, China

Supporting Information

ABSTRACT: Long-chain L-α-hydroxy acid oxidase (LCHAO) is a flavin mononucleotide (FMN)-dependent oxidase that dehydrogenates L-α-hydroxy acids to keto acids. There were two different mechanisms, named as hydride transfer (HT) mechanism and carbanion (CA) mechanism, respectively, proposed about the catalytic process for the FMN-dependent L-α-hydroxy acid oxidases on the basis of biochemical data. However, crystallographic and kinetic studies could not provide enough evidence to prove one of the mechanisms or eliminate the alternative. In the present studies, theoretical computations were carried out to study the molecular mechanism for LCHAO-catalyzed dehydrogenation of L-lactate. Our molecular dynamics (MD) simulations indicated that L-lactate prefers to bind with LCHAO in a hydride transfer mode rather than a carbanion mode. Quantum mechanics/molecular mechanics (QM/MM) calculations were further carried out to obtain the optimized structures of reactants, transition states, and products at the level of ONIOM-EE (B3LYP/6-311++G(d,p)//B3LYP/6-31G(d,p):AMBER). Quantum chemical studies indicated that LCHAO-catalyzed dehydrogenation of L-lactate would be a stepwise catalytic reaction in a hydride transfer mechanism but not a carbanion mechanism. MD simulations, binding free energy calculations, and QM/MM computations were also implemented on the complex between L-lactate and Y129F mutant LCHAO. By comparing the Y129F mutant system with the wild-type system, it was further confirmed that the key residue Tyr129 in the active site of LCHAO would not affect L-lactate's binding to LCHAO but play an important role on the catalytic reaction process through an H-bond interaction.

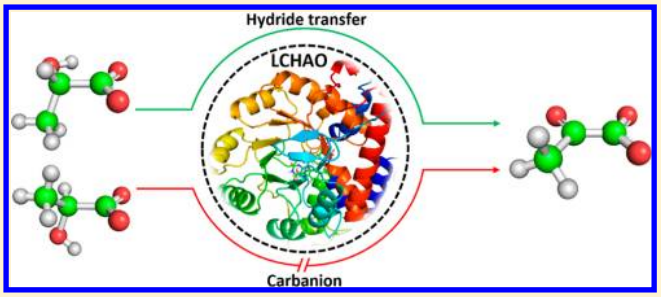

INTRODUCTION

Long-chain L-α-hydroxy acid oxidase (LCHAO) is a peroxisomal enzyme (EC 1.1.3.15, isozyme B) mainly obtained from rat liver and kidney. LCHAO was first identified to be active for some natural amino acids.[1] Subsequently, it was also found to oxidize a large variety of L-α-hydroxy acids such as L-lactate and L-α-hydroxy isocaproate at the expense of oxygen.[2] There are two forms of LCHAO, subtypes β1 and β2, identified with the cloning and sequencing of their cDNAs. The sequence-longer subtype β2 differs from β1 in having a three-residue insertion, -VRK-, from position 188 to 189 in the loop 4 of the mature subtype β1. The subtype β1 represents for nearly 90% of the protein expressed in rat liver.[3] LCHAO was also discovered to oxidize creatol with formation of methylguanidine in rat kidney,[4,5] which is a toxic compound with elevating serum levels in patients with chronic renal failure.[6,7] Inhibitors of LCHAO may thus be capable of taking effect in uraemia.[8]

LCHAO is a member of a well-characterized FMN-dependent L-α-hydroxy acid oxidase enzyme family, which includes yeast flavocytochrome b_2 (FCB2),[9] mandelate dehydrogenase from *Pseudomonas putida* (MDH),[10] spinach glycolate oxidase (GOX),[11] human glycolate oxidase (hGOX, encoded by *HAOX1* gene),[12] human L-α-hydroxy acid oxidase 2 (HAOX2, encoded by *HAOX2* gene),[13] and mouse L-α-hydroxy acid oxidase 3 (HAOX3, encoded by *HAOX3* gene).[13] Among these isozymes, HAOX2 is most similar to LCHAO, having a sequence identity of 74% with each other. The reported crystal structures of LCHAO[8,14] clearly show that LCHAO has very similar three-dimensional configurations with an identical $\beta_8\alpha_8$ barrel fold in comparison with other structurally characterized family members (Figure S1 in the Supporting Information). As shown in Figures S1 and S2 in the Supporting Information, residues Phe23, Tyr129, Asp157, Arg164, Lys223, His247, and Arg250 in the active site of LCHAO are well conserved among the FMN-dependent L-α-hydroxy acid oxidase enzyme family. A loop region, known as loop 4, situated between β-strand 4 and α-helix 4 of the TIM barrel is disordered in nearly all of the known crystal structures of the enzyme family, indicating a high variability of this part.

The catalytic cycle involving an FMN-dependent L-α-hydroxy acid oxidase encloses two steps, a flavin-reductive half-reaction and subsequently a flavin-oxidative half-reaction[15] (Scheme 1). In the former step, a substrate L-α-hydroxy acid undergoes an oxidation by transferring two electrons to flavin

Received: March 4, 2014
Revised: May 4, 2014
Published: May 6, 2014

dx.doi.org/10.1021/jp5022399 | J. Phys. Chem. B 2014, 118, 5406−5417

Scheme 1. Catalytic Cycle of FMN-Dependent L-α-Hydroxy Acid Oxidases

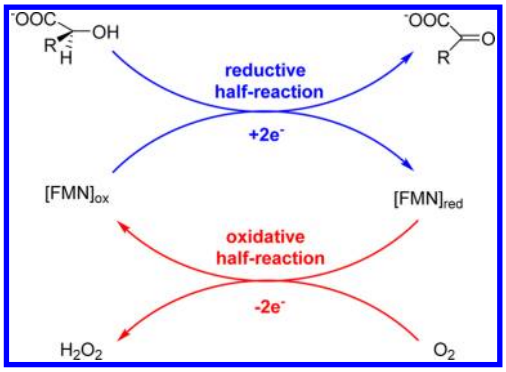

mononucleotide (FMN) which is reduced to hydroquinone. In the latter step, FMN is reoxidized by an electron acceptor such as oxygen. Due to the highly homologous tertiary structure and conserved residues in the active sites of L-α-hydroxy acid oxidases, flavin-reductive half-reaction could proceed in an identically catalytic mechanism. However, there are different mechanisms proposed to the flavin-oxidative half-reaction for the family members.[14,16,17] In the present work, we will focus on computational studies of the catalytic mechanism in the reductive half-reaction part, which was thought to be more important step in the enzyme-catalyzed oxidations of L-α-hydroxy acids.[18]

There are two different mechanisms suggested for the reductive half-reaction step on the basis of biochemical studies.[15] In the first proposed mechanism named as hydride transfer (HT) (Figure 1a), the α-hydroxyl proton of a binding substrate would be transferred to a base group in the active site of enzyme, promoting the transport of its α-hydrogen to FMN to produce a keto acid. In an alternative one named as a carbanion (CA) mechanism (Figure 1b), the reaction was predicted to proceed through the formation of an intermediate carbanion generated by an active-site base abstracting the α-proton of a binding substrate. However, the dispute of the correct mechanism remains unsolved up to the present.[20,21] In the active site of the enzyme, the imidazole side chain of a highly conserved residue histidine, which is close to the isoalloxazine part of FMN, has been proposed to be a base group that initiates the enzyme-catalytic reaction. The inconsistency between these two suggested mechanisms originates from different orientations of the α-hydroxyl group or the α-hydrogen of a substrate L-α-hydroxy acid in the active site of enzyme. In the binding mode for the proposed HT mechanism, the α-hydroxyl group would form a hydrogen bond with NE2 atom of His247 (in LCHAO) to have the α-hydrogen point toward the N5 atom of FMN. Such a binding mode is regarded as an HT mode. In contrast, the α-hydrogen of substrate points to the NE2 atom of His247, thus leaving the α-substituted bulky group close to FMN and Ala78 (in LCHAO) in its binding mode, called as a CA mode, for the assumed CA mechanism.

The chemical mechanism for L-α-hydroxy acid's dehydrogenation catalyzed by an FMN-dependent L-α-hydroxy acid oxidase has long been considered to involve the initial formation of a carbanion (CA mechanism) via the catalytic histidine abstracting the substrate C2 hydrogen as a proton.[22−24] The mechanism was proposed on the fact that the catalytic His is in an appropriate position for α-proton abstraction in the catalytic center.[15] The produced dianionic intermediate of the substrate could be stabilized by forming salt bridge interactions with positively charged residues Arg164, Arg250, and His247 (in LCHAO). Dewanti et al.[24] reported a transient intermediate formed in the step of FMN reduction reaction. This intermediate was identified to be a charge-transfer complex of oxidized FMN and an electron-rich donor and was suggested to be a carbanion/enolate intermediate generated by base-promoted abstraction of the substrate α-proton. However, such a finding was also in line with the existence of an electron-rich deprotonated alkoxide intermediate, formed by α-hydroxyl deprotonation of L-lactate, as proposed by Fitzpatrick et al.[25,26] To the best of our knowledge, the whereabouts of the substrate's α-hydroxyl proton was not explained yet in the proposed CA mechanism,[15,19] which may be lost into the solvent.

Site-directed mutagenesis seems to indirectly support the assumed CA mechanism. An FCB2 double mutant A198G/L230A had a 400-fold increased rate with L-mandelate, but a low rate and a reduced efficiency with L-lactate.[27,28] This would be consistent with the presumption that the relived steric hindrance will make L-mandelate easier to orientate correctly in

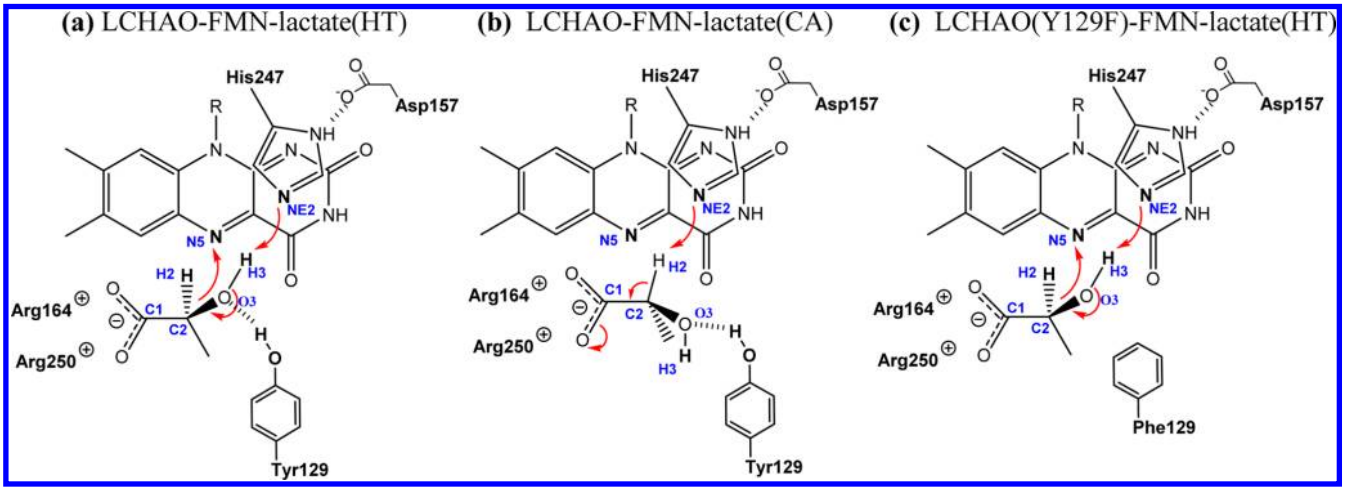

Figure 1. Proposed[15] (a) HT mechanism and (b) CA mechanism of L-lactate oxidation by WT LCHAO and (c) HT mechanism for Y129F mutant LCHAO.

dx.doi.org/10.1021/jp5022399 | J. Phys. Chem. B 2014, 118, 5406−5417

the CA mode while only decrease the binding affinity of smaller L-lactate. On the other hand, molecular modeling indicated that a hydride transfer would occur since the bulky phenyl group of L-mandelate would prevent its binding in the active site of FCB2 with an appropriate orientation for α-proton abstraction by His373 (FCB2).[29] Cunane et al.[14] also found it possible to build a satisfactory model for HT but not CA mechanism. Unfortunately, researchers have not reached an agreement on this contentious topic over the decades. This could be partly attributed to the fact that the crystallographic and kinetic studies could not provide enough evidence to prove one of the mechanisms or eliminate the alternative. Another reason is probably that the transition state in the reaction is difficulty to be identified by traditional experimental methods.

Computational means, like quantum mechanics/molecular mechanics (QM/MM) approach, have been widely applied for studying kinetic mechanisms for enzyme-catalyzed reactions.[30−33] Molecular dynamics (MD) simulations, which were widely used[34−37] to simulate interaction features for a ligand or substrate binding to its target protein, could be implemented to study the favorable binding mode of L-α-hydroxy acid in the active site of enzyme. Nevertheless, to the best of our knowledge, no detailed and systematic calculations have been carried out to study the reaction mechanism of L-α-hydroxy acid dehydrogenation catalyzed by LCHAO. In fact, some basic models using different substrates and specific enzyme crystal structure[14,29,38] did not convincingly elucidate the preferable binding mode and did not refer to the reaction kinetics.

In the present work, computational studies were performed on two different proposed reaction mechanisms, i.e., HT and CA mechanisms, via MD simulations and QM/MM calculations of LCHAO-catalyzed dehydrogenation of L-lactate. L-Lactate is a typical substrate of LCHAO and other isozymes in the family of FMN-dependent L-α-hydroxy acid oxidases. At first, MD simulations were carried out to figure out a preferable binding mode for LCHAO-catalyzed oxidation reaction of L-lactate to produce pyruvate. In the meantime, the Y129F mutant LCHAO model was also built to investigate the effects of the key residue Tyr129 on the binding of L-lactate and LCHAO-catalyzed oxidation reaction, since biochemical data[38,39] indicated that this highly conserved residue had no influence on the binding affinity of a substrate but had great effects on the enzyme-catalyzed oxidation rate. These could be important clues to identify the preferable reaction mechanism. Furthermore, QM/MM computations were executed to discover the transition states of LCHAO-catalyzed oxidation reaction of L-lactate on the basis of MD-simulated structural models of L-lactate binding to LCHAO or its mutant Y129F. Our quantum chemical calculations not only proposed a preferred reaction mechanism for the LCHAO-catalyzed oxidation reaction of L-lactate to produce pyruvate but also predicted the effects of the key residue Tyr129 on the reaction transition states.

COMPUTATIONAL DETAILS

Initial Structure Preparation. The high-resolution X-ray cocrystal structure of rat LCHAO in complex with FMN and its inhibitor 4-carboxy-5-[(4-chlorophenyl)sulfanyl]-1,2,3-thiadiazole (CCPST) was downloaded from the Protein Data Bank (PDB entry: 3SGZ[8]). Since the residues Leu183-Val197 in loop 4 are missing in the cocrystal structure, we first supplied the coordinates of Leu183-Val197 using a web server ModLoop[40] for modeling of loop in the protein structure. The crystal water molecules presented in the PDB file were kept. The crystal structure of L-lactate[41] was obtained from the International Union of Crystallography (http://journals.iucr.org/) to be regarded as the initial structure of the substrate. L-Lactate was merged into the above cocrystal structure 3SGZ to replace the ligand CCPST for the generation of initially structural models of the complex LCHAO-FMN-lactate. For such a purpose, the carboxylate and C2 atoms of L-lactate were superimposed onto the corresponding atoms of CCPST to get an initial model of LCHAO-FMN-lactate(HT) (Figure 1a) for the computational studies of the HT mechanism. For the computational studies of the CA mechanism, another initial model of LCHAO-FMN-lactate(CA) (Figure 1b) was obtained by manually rotating the bond C1−C2 of L-lactate by 100° to make the α-hydrogen point toward the NE2 atom of His247 for α-proton abstraction. Furthermore, the third initial model of LCHAO(Y129F)-FMN-lactate(HT) (Figure 1c) was also generated to explore the effect of the key residue Tyr129 in the active site of LCHAO by in silico mutating Tyr129 to Phe on the basis of initially structural model of LCHAO-FMN-lactate(HT).

MD Simulations. Molecular dynamics simulations were first carried out on the above three complexes using AMBER12 software package.[42] Protonation states of charged residues and histidines were assigned on the basis of pK_a values calculated by PROPKA.[43] All missing hydrogen atoms were added using the LEaP module[44] in AMBER 12. A periodic truncated octahedron box of TIP3P water molecules with a margin distance of 9.0 Å was created around each complex which was neutralized by one additional Na^+. The restrained electrostatic potential (RESP) charges were treated as the partial atomic charges for L-lactate and FMN by fitting the electrostatic potentials calculated by GAUSSIAN 09[45] at the HF/6-31G* level of theory. The general AMBER force field (GAFF) was assigned to establish the force filed parameters of L-lactate and FMN, while the AMBER ff99SB force field was assigned for the potential of LCHAO, water molecules, and Na^+. The missing parameters of FMN were obtained from an AMBER parameter database contributed by Schneider et al.[46] at the web site http://www.pharmacy.manchester.ac.uk/bryce/amber.

Prior to MD simulations, each system was subjected to a three-step energy minimization for the relaxation of any steric conflicts produced during system setup. First, all Na^+ and water molecules were optimized with the fix of atoms from LCHAO, FMN, and L-lactate. The second minimization step was run with a constraint force of 5.0 kcal/(mol·Å^2) to restrain the heavy atoms of residues Leu183 to Val197 built by ModLoop[40] and with the fix of the heavy atoms from L-lactate, FMN, and residues Phe23, Ala78, Tyr107, Tyr129, Asp157, Arg164, Lys223, His247, and Arg250 around the active pocket of LCHAO. Finally, the whole system was optimized without any restraint. In each above step, structural optimization was implemented using 2500 steps of steepest descent followed by 5000 steps of conjugate gradient method. After energy minimizations, each system was then gradually heated in the NVT ensemble from 0 to 300 K over 100 ps with force constants of 500 kcal/(mol·Å^2) on L-lactate, FMN, and residues in the active site and 10 kcal/(mol·Å^2) on other residues of LCHAO. Subsequently, two rounds of 10 ns MD equilibrations followed by another 20 ns MD productions were run with a periodic boundary condition in the NPT ensemble at 300 K. In the first round of 10 ns MD equilibrations, the heavy atoms of FMN, L-lactate, and residues in the active site of LCHAO were

dx.doi.org/10.1021/jp5022399 | J. Phys. Chem. B 2014, 118, 5406−5417

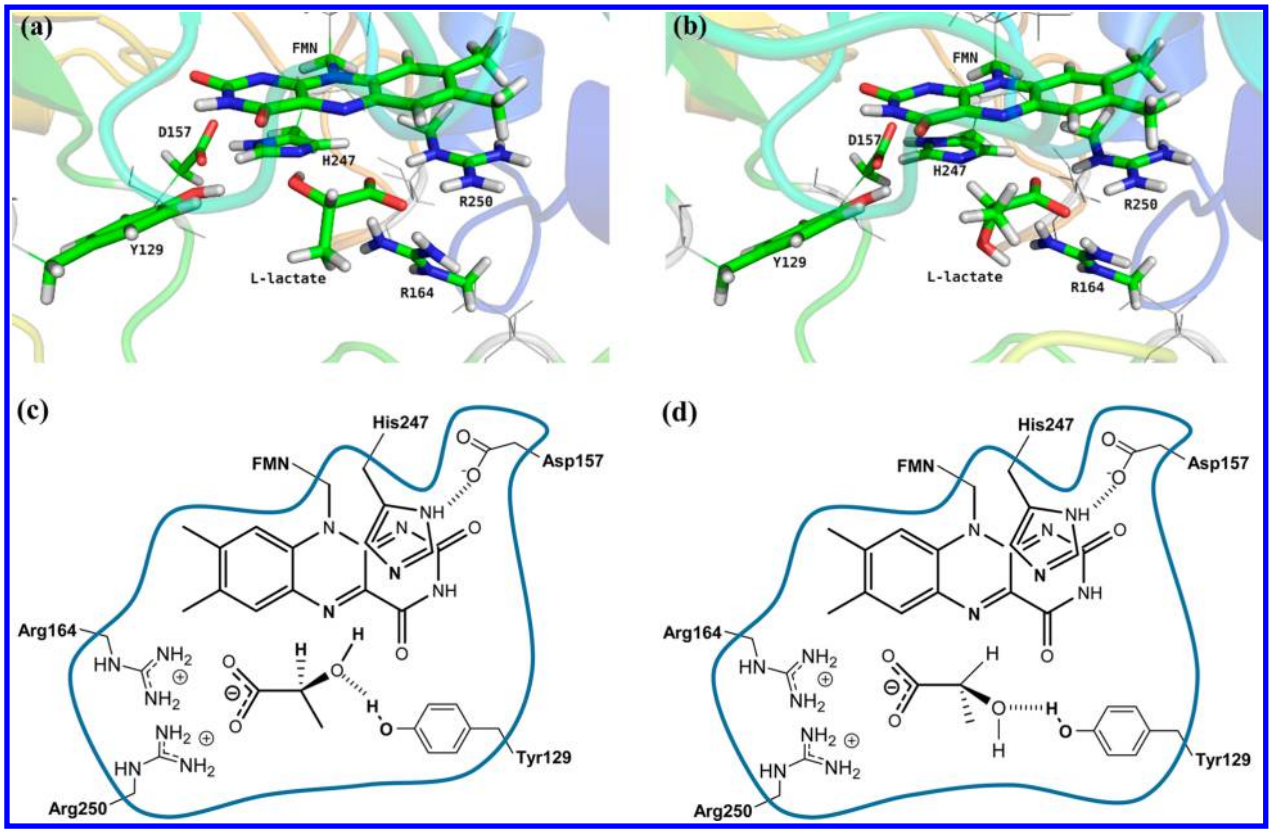

Figure 2. (a,c) HT and (b,d) CA models considered during the ONIOM calculations. Atoms shown as sticks in (a) and (b) are treated as QM layer, while the rest are set as MM layer. Atoms inside the boxes in (c) and (d) are treated as QM layer, while the rest are set as MM layer.

fixed and the heavy atoms of other residues were imposed with a force constraint of 5 kcal/(mol·Å^2). The second 10 ns MD equilibrations were run with only fixing heavy atoms of substrates and active site residues of LCHAO. Finally, the whole system was run for 20 ns MD productions without any force constraint. During the whole 40 ns MD simulations, particle-mesh Ewald (PME)[47] was employed to deal with the long-range electrostatic interactions. A 10 Å cutoff distance was used for the long-range van der Waals (vdW) energy term. SHAKE algorithm[48] was employed to keep all bonds involving hydrogen atoms rigid. The trajectories were recorded every 1 ps.

Binding Free Energy Calculations and Per-Residue Free Energy Decomposition Analyses. To check the effect of Tyr129 on L-lactate's binding affinity, 400 snapshots were extracted from the last 4 ns MD simulations of complex LCHAO-FMN-lactate(HT) or LCHAO(Y129F)-FMN-lactate-(HT) at 10 ps intervals to estimate the binding free energy of L-lactate with either LCHAO or Y129F mutant LCHAO using the molecular mechanics/generalized Born surface area (MM/GBSA) method.[49] Moreover, the binding free energies were decomposed to each residue's contribution to ligand using the MM/GBSA[49] decomposition process in AMBER 12[42] in order to explore the interactions of L-lactate with each residue around the active sites of LCHAO or its mutant Y129F more deeply. The binding free energy calculations and per-residue free energy decompositions followed the approaches as described in our previous publication.[50]

QM/MM Calculations. The last snapshot of the second round 10 ns MD equilibrations (with only heavy atoms of active site and substrates fixed) of each system was selected as the initial structure for QM/MM calculations. In order to eliminate some improper distortions, three steps of energy minimizations were first conducted following same procedure as described in the section MD Simulations. Subsequently, water molecules that are either within 3 Å around the enzyme or within 15 Å around the active center (Phe23, Tyr129, Asp157, Arg164, Lys223, His247, Arg250, FMN, and L-lactate) were kept, while others were erased to reduce the sizes of models. The treated LCHAO-FMN-lactate(HT), LCHAO-(Y129F)-FMN-lactate(HT), and LCHAO-FMN-lactate(CA) systems have about 9870 atoms for their QM/MM computations.

A two-layer ONIOM method in GAUSSIAN 09,[45] which has been widely applied in enzyme systems,[31,51−53] was implemented for all QM/MM calculations. As illustrated in Figure 2, the isoalloxazinyl ring of FMN, all atoms of L-lactate, and part of side chains of residues Tyr129, Asp157, Arg164, His247, and Arg250 of LCHAO were included in the QM region of system. This high-level layer was composed of 103 atoms including 6 hydrogen link atoms employed to treat the QM/MM boundary. The remaining atoms were included in the MM part of system. The total charge was −1 for the whole real system and 0 for model system.

Optimized stationary points including minima and transition states (TS) were obtained at the B3LYP/6-31G(d,p) level of theory for the QM layer, and AMBER96 force field for the MM layer. An electronic embedding (EE) scheme[54] was applied to provide a better description of the electrostatic interaction between QM and MM regions. During QM/MM optimizations, residues more than 6 Å away from the active center (Phe23, Tyr129, Asp157, Arg164, Lys223, His247, Arg250,

dx.doi.org/10.1021/jp5022399 | J. Phys. Chem. B 2014, 118, 5406−5417

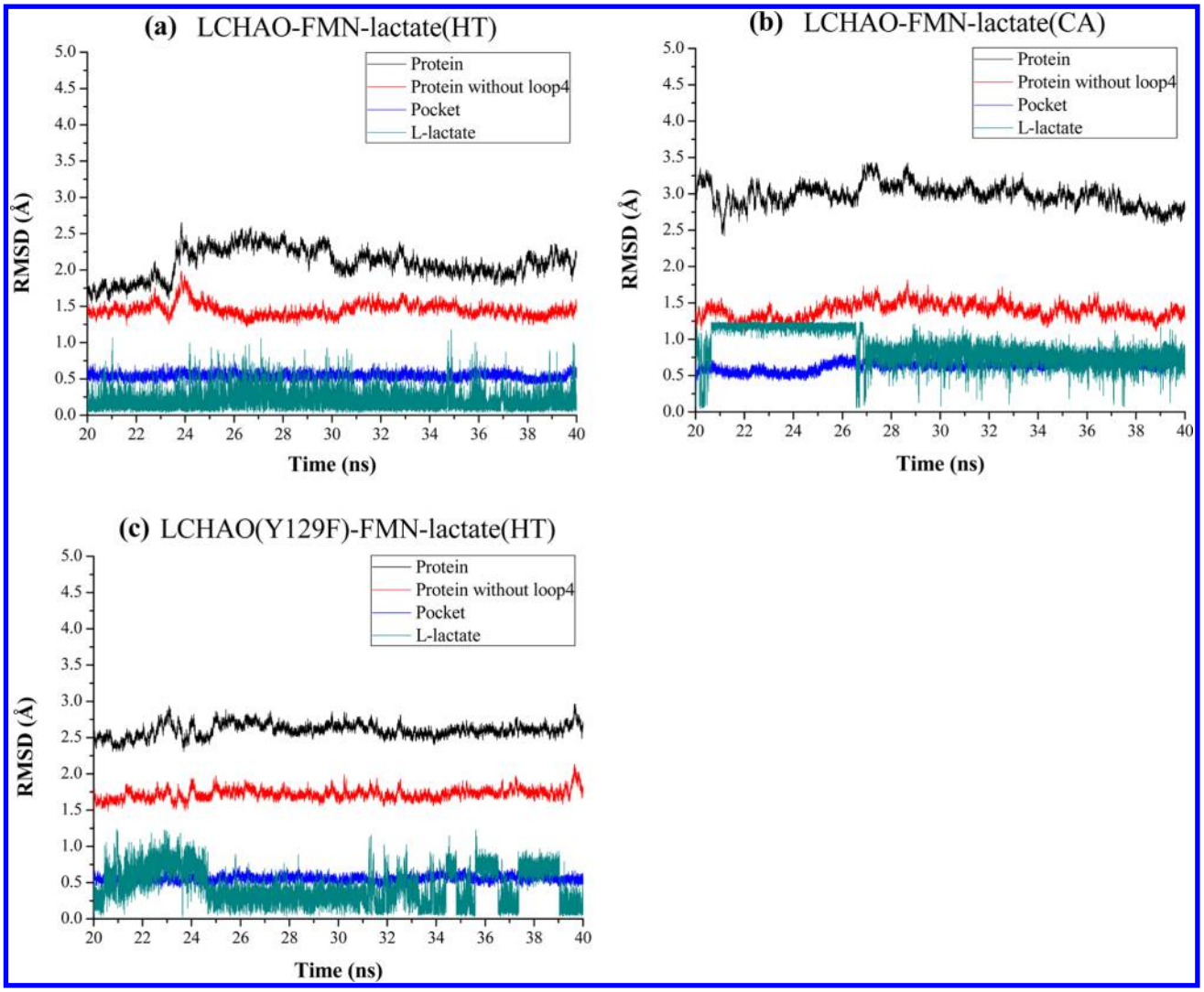

Figure 3. Rmsds of backbone atoms (C, Cα, and N) of protein, backbone atoms of protein without loop 4, backbone atoms of binding pocket (within 6.5 Å), and heavy atoms of L-lactate for (a) HT model of the WT, (b) CA model of the WT, and (c) HT model of Y129F mutant during last 20 ns (out of 40 ns) MD simulations.

FMN, and L-lactate) were held fixed. Analytic frequency calculations at the same level of theory as applied in the geometry optimizations were conducted to confirm the minima (zero imaginary frequencies) or TS (only one imaginary frequency). The thermal correction to Gibbs free energy was also obtained from each frequency calculation. Refined structures were finally subjected to single-point energy calculations at the ONIOM (B3LYP/6-311++G(d,p):AMBER) level of theory. To check the sensitivity of the results to the choice of functional, further single-point calculations were done using the ωB97X and ωb97XD methods. To make the reaction energy profile more reliable, the free energy of each stationary point was last estimated as the sum of the total electronic energy (single-point energy) obtained at the higher level and the corresponding thermal correction to Gibbs free energy.

RESULTS AND DISCUSSION

MD Simulations of HT and CA Models of L-Lactate Binding to LCHAO. 40 ns molecular dynamics simulations were carried out on systems LCHAO-FMN-lactate(HT) and LCHAO-FMN-lactate(CA), respectively, to explore the interaction modes of substrate L-lactate binding to LCHAO for its dehydrogenation in an HT mode or CA mode. In each case, the first 20 ns were run for equilibriums of the enzyme and the last 20 ns were run to examine the binding stability and characteristics without constraints. Figure 3 illustrates the root-mean-square deviations (rmsds) of the last 20 ns MD productions relative to the starting structure. In each case, rmsd of protein became lower and more stable when loop 4 was excluded from the analysis. This phenomenon implied that loop 4 possessed a high variability, which is consistent with crystallography studies.[8,14] Moreover, the binding pocket defined to enclose residues within 6.5 Å around L-lactate remained stable during the last 20 ns MD productions, with the backbone fluctuating at around 0.5 Å. This somehow verified the rationality of obtained trajectories.

On the other hand, rmsds of heavy atoms of L-lactate revealed that the substrate suffered a different conformational change during the computational time in the MD-simulated complexes LCHAO-FMN-lactate(HT) (Figure 3a) and LCHAO-FMN-lactate(CA) (Figure 3b). As shown in Figure 3a, L-lactate remained stable during the last 20 ns production period of MD simulations with rmsd values of about 0.2 Å in the complex LCHAO-FMN-lactate(HT) for later QM/MM

dx.doi.org/10.1021/jp5022399 | J. Phys. Chem. B 2014, 118, 5406−5417

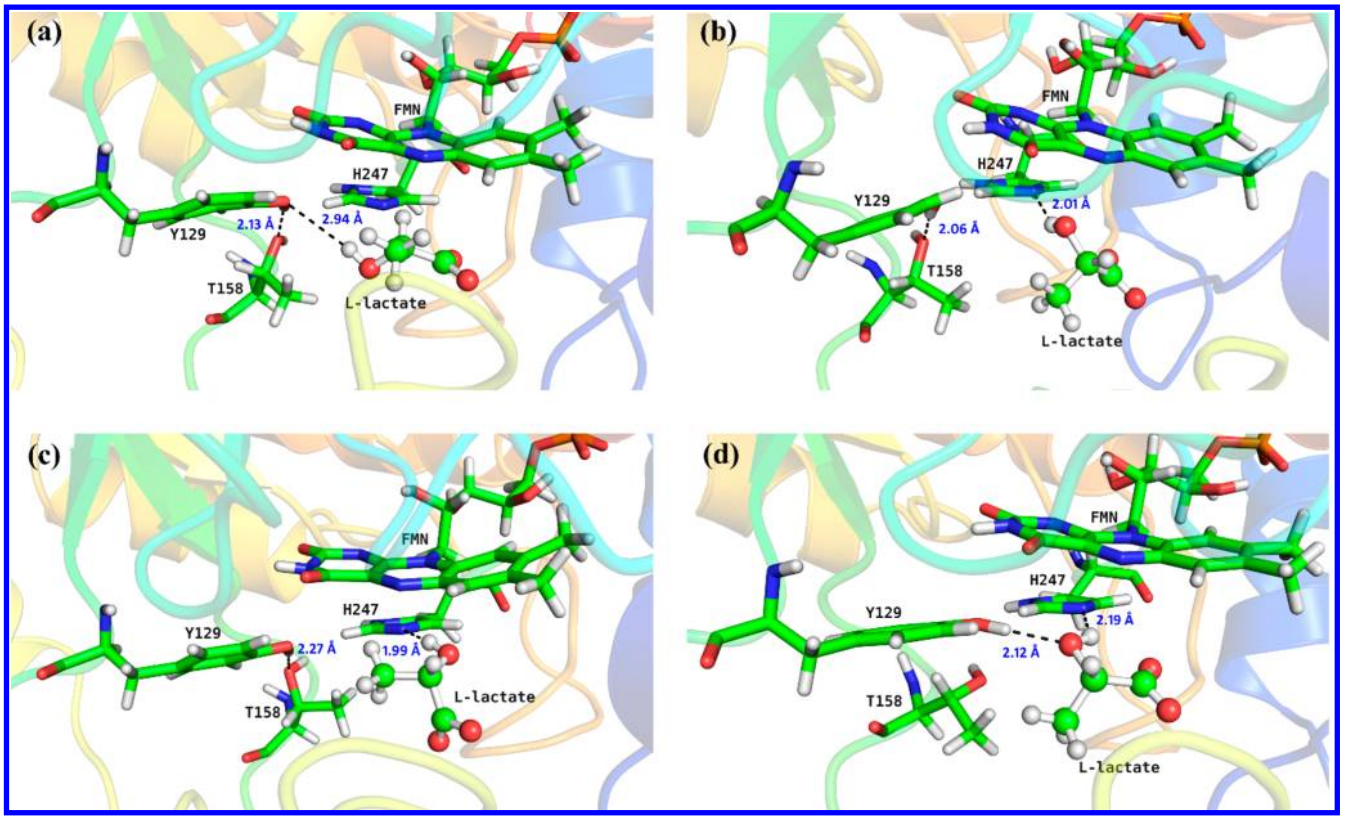

Figure 4. Different binding conformations of L-lactate during the free MD simulations (last 20 ns) in the case of CA mode: (a) conformation **1** at the beginning of production phase; (b) conformation **2** after 50 ps; (c) conformation **3** after 1 ns; (d) conformation **4** after 7 ns. L-Lactate is shown as ball and sticks.

calculations of an HT mechanism. The trajectory indicated that the interactions between L-lactate and residues in the active site of LCHAO were stable during the vast majority of time. Moreover, the hydride binding mode of L-lactate with LCHAO maintained until the end of MD simulations. Conversely, it was noted that L-lactate changed its binding conformation several times during the last 20 ns MD simulations in the case of LCHAO-FMN-lactate(CA) for a proposed binding mode for the LCHAO-catalyzed oxidation reaction of L-lactate in a CA mechanism (Figure 3b). Once the restraint was released, the rmsds of L-lactate fluctuated dramatically. As shown in Figure 4a, at the beginning of MD productions of LCHAO-FMN-lactate(CA), α-OH of L-lactate (conformation **1**) formed a hydrogen bond (2.94 Å, 173.0°) with the phenolic hydroxyl oxygen of Tyr129, which donated another hydrogen bond (2.13 Å, 152.7°) to the side-chain OH of Thr158. After 50 ps of nonrestraint MD simulations of CA model, it was observed that L-lactate (conformation **2,** Figure 4b) had its α-OH pointing to the NE2 atom of His247, making the substrate ready for the LCHAO-catalyzed oxidation reaction of L-lactate in the HT mechanism. The structure of L-lactate altered significantly after that it remained stable at conformation **3** (Figure 4c) during 1 to 6.5 ns. After 7 ns of MD productions until the end of the simulations, L-lactate was changed to conformation **4** (Figure 4d) which is actually a standard conformation in the HT binding mode. Our MD simulations indicated that the initial binding carbanoin mode LCHAO-FMN-lactate(CA) would be not stable for L-lactate to interact with residues in the active site of LCHAO.

During MD simulations, Tyr129 changed from the hydrogen bond acceptor to donor after 7 ns MD productions of LCHAO-FMN-lactate(CA), which showed a similar interaction to the α-hydroxyl group of L-lactate in MD-simulated LCHAO-FMN-lactate(HT) for the HT mechanism. It could be possible that Tyr129 plays a key role in the structure alteration process in the MD simulations of LCHAO-FMN-lactate(CA). The hydrogen bond formed between the phenolic hydroxyl oxygen of Tyr129 and α-OH of L-lactate could act as a "driving force" to prompt the rotation of bond C1−C2 to make α-H of L-lactate point toward N5 of FMN and its α-OH stay closer to His247. As discussed later, MD simulations were also performed on the interaction mode of L-lactate binding to Y129F mutant LCHAO to explore the effects of Tyr129 on the binding substrate. In addition, in the case of the initial CA mode, L-lactate had its α-OH group point toward a hydrophobic pocket formed by Leu161, Pro196, Phe199, and the side-chain methyl group of Thr158 of LCHAO. Such an unfavorable interaction was believed to be unstable in the MD simulations of LCHAO-FMN-lactate(CA), but the corresponding hydrophobic pocket could stabilize the methyl group of L-lactate in LCHAO-FMN-lactate(HT).

Above all, the MD results may indicate that the initially generated model of LCHAO-FMN-lactate(CA) would not be suitable for the LCHAO-catalyzed oxidation reaction of L-lactate in a proposed CA mechanism, and L-lactate would transfer to a conformation in the binding mode like LCHAO-FMN-lactate(HT) for the HT mechanism during MD simulations. Accordingly, the MD-simulated interaction mode of L-lactate binding to LCHAO would be preferable for an HT mode rather than a CA mode. In fact, Sukumar et al.[55] found the ligand may exist in a mixture of keto acid product and hydroxyl acid with the HT mode in the cocrystal structure of 2-

dx.doi.org/10.1021/jp5022399 | J. Phys. Chem. B 2014, 118, 5406−5417

Table 1. MM/GBSA Binding Free Energies and Energy Components between L-Lactate and LCHAO in the HT Mode (in kcal/mol)

system	ΔE_{vdW}[a]	$\Delta G_{nonpol,sol}$[b]	ΔE_{ele}[c]	$\Delta G_{ele,sol}$[d]	ΔG_{np}[e]	ΔG_{ele}[f]	$T\Delta S$[g]	ΔG_{bind}[h]
WT	−9.66	−2.10	−150.51	121.64	−11.76	−28.87	−13.48	−27.15
Y129F	−9.88	−2.09	−162.98	133.43	−11.97	−29.55	−13.89	−27.63

[a]The van der Waals energy component. [b]The nonpolar contribution to the solvation free energy. [c]The electrostatic interaction energy between the substrate and enzyme. [d]The polar contribution to the solvation free energy. [e]The nonpolar component of the enzyme−substrate binding free energy. $\Delta G_{np} = \Delta E_{vdW} + \Delta G_{nonpol,sol}$. [f]The electrostatic component of the enzyme−substrate binding free energy. $\Delta G_{ele} = \Delta E_{ele} + \Delta G_{ele,sol}$ [g]The conformational entropy term obtained by using the NMODE[59] module on 40 snapshots taken from the last 4 ns of the MD trajectory. [h]The total binding free energy. $\Delta G_{bind} = \Delta E_{vdW} + \Delta G_{nonpol,sol} + \Delta E_{ele} + \Delta G_{ele,sol} - T\Delta S$.

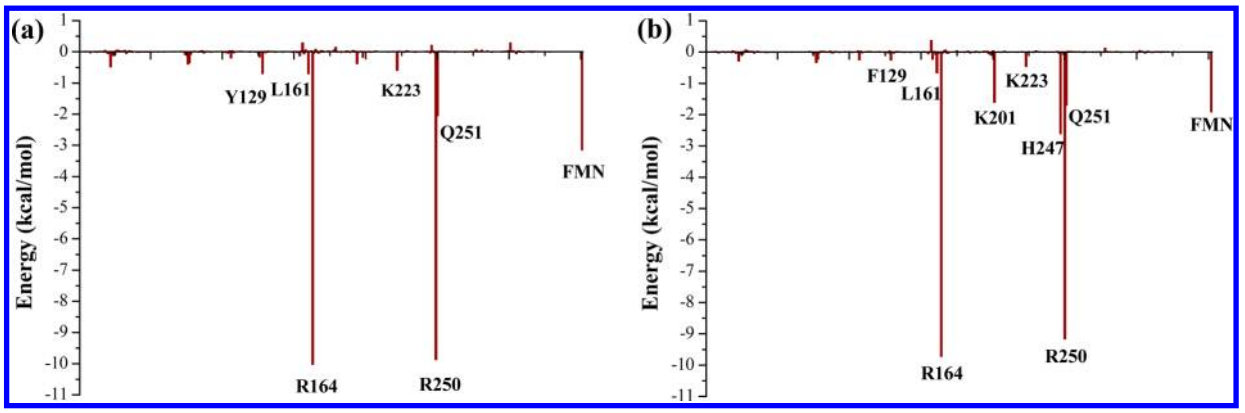

Figure 5. Per-residue energy decomposition of L-lactate binding with (a) WT LCHAO and (b) Y129F mutant LCHAO both in HT conformation.

hydroxyoctanoate with G81A mutant MDH which is an isozyme of LCHAO.

MD Simulations of HT Model of Y129F Mutant LCHAO. The residue Tyr129 of LCHAO is a highly conserved residue in the active sites of FMN-dependent L-α-hydroxy acid oxidases. The mutations of corresponding conserved Tyr to Phe in FCB2[38] and GOX[39] resulted in significantly decreased k_{cat} values ($k_{cat}^{WT\ FCB2} = 270\ s^{-1}$ versus $k_{cat}^{Y254\ mutant\ FCB2} = 6.10\ s^{-1}$ and $k_{cat}^{WT\ GOX} = 25\ s^{-1}$ versus $k_{cat}^{Y129F\ mutant\ GOX} = 0.63\ s^{-1}$) but no change of the respective K_m values ($K_m^{WT\ FCB2} = 0.49$ mM versus $K_m^{Y254F\ mutant\ FCB2} = 0.35$ mM and $K_m^{WT\ GOX} = 0.94$ mM versus $K_m^{Y129F\ mutant\ GOX} = 1.0$ mM). As an isozyme to these two FMN-dependent L-α-hydroxy acid oxidases, it may be hypothesized that LCHAO could have similar characteristics for the highly conserved Tyr129. Therefore, we performed MD simulations on a generated interaction model of L-lactate binding to the Y129F mutant LCHAO on the basis of the initial structure of complex LCHAO-FMN-lactate(HT) to explore the role of Tyr129 in the binding state of L-lactate with LCHAO. As illustrated in Figure 3c, the system LCHAO-FMN-lactate-(Y129F) achieved equilibrium after 5 ns of nonrestrained MD simulations, shown by the stable rmsd values of the protein and pocket. In comparison with MD simulated LCHAO-FMN-lactate(HT), the carboxyl group of L-lactate move slightly away from Arg164 and Arg250, forming an extra H-bond interaction with the side chain of K201 in MD-simulated LCHAO-(Y129F)-FMN-lactate. This could be attributed to the loss of the hydrogen bond between Phe129 and α-OH of L-lactate, which may induce the substrate to be more flexible. Nevertheless, it was observed that the HT mode was maintained during MD simulations, with α-OH of L-lactate pointing to NE2 atom of His247 and α-H of L-lactate pointing to the N5 atom of FMN. However, the distance between the α-H of L-lactate and N5 atom of FMN became about 0.65 Å longer in the case of LCHAO(Y129F)-FMN-lactate(HT) (3.58 Å on average in the last 20 ns MD) as compared to LCHAO-FMN-lactate(HT) (2.93 Å on average in the last 20 ns MD), indicating that Tyr129 in WT LCHAO is important to maintain the near attack conformation (NAC)[56] of the reaction center for the HT process to proceed. The binding free energies were further calculated to investigate whether the binding free energy has been affected by a little change of the bind mode upon Tyr129 mutation.

Binding Free Energies and Energy Decomposition Analyses. Table 1 lists the calculated binding free energies and their components of L-lactate in the complexes LCHAO-FMN-lactate(HT) and LCHAO(Y129F)-FMN-lactate(HT) using MM/GBSA method based on the last 4 ns trajectories of MD simulations. As discussed above, it was observed that the binding conformation of L-lactate in LCHAO-FMN-lactate-(CA) could automatically change to the one like in LCHAO-FMN-lactate(HT) during MD simulations. Therefore, the binding free energy was not further computed in the case of LCHAO-FMN-lactate(CA). It can be seen that the binding free energies (ΔG_{bind}) of L-lactate in both LCHAO-FMN-lactate-(HT) and LCHAO(Y129F)-FMN-lactate(HT) are nearly same with the values of −27.15 and −27.63 kcal/mol, respectively. Both nonpolar contribution ($\Delta G_{np} = \Delta E_{vdW} + \Delta G_{nonpol,sol}$) and polar contribution ($\Delta G_{ele} = \Delta E_{ele} + \Delta G_{ele,sol}$) in the case of WT enzyme−substrate (−11.76 and −28.87 kcal/mol, respectively) are close to those of mutant−substrate (−11.97 and −29.55 kcal/mol, respectively). These results indicated that the mutation Y129F would not affect the L-lactate's K_m with LCHAO. In fact, biochemical studies have demonstrated that L-lactate has similar K_m values in WT GOX and Y129F mutant GOX.[39]

Per-residue energy decomposition was further conducted to explore the reason why no variation of the substrate's binding affinity could be observed for Y129F mutant LCHAO as compared to WT LCHAO. As shown in Figure 5, Tyr129 and

dx.doi.org/10.1021/jp5022399 | J. Phys. Chem. B 2014, 118, 5406−5417

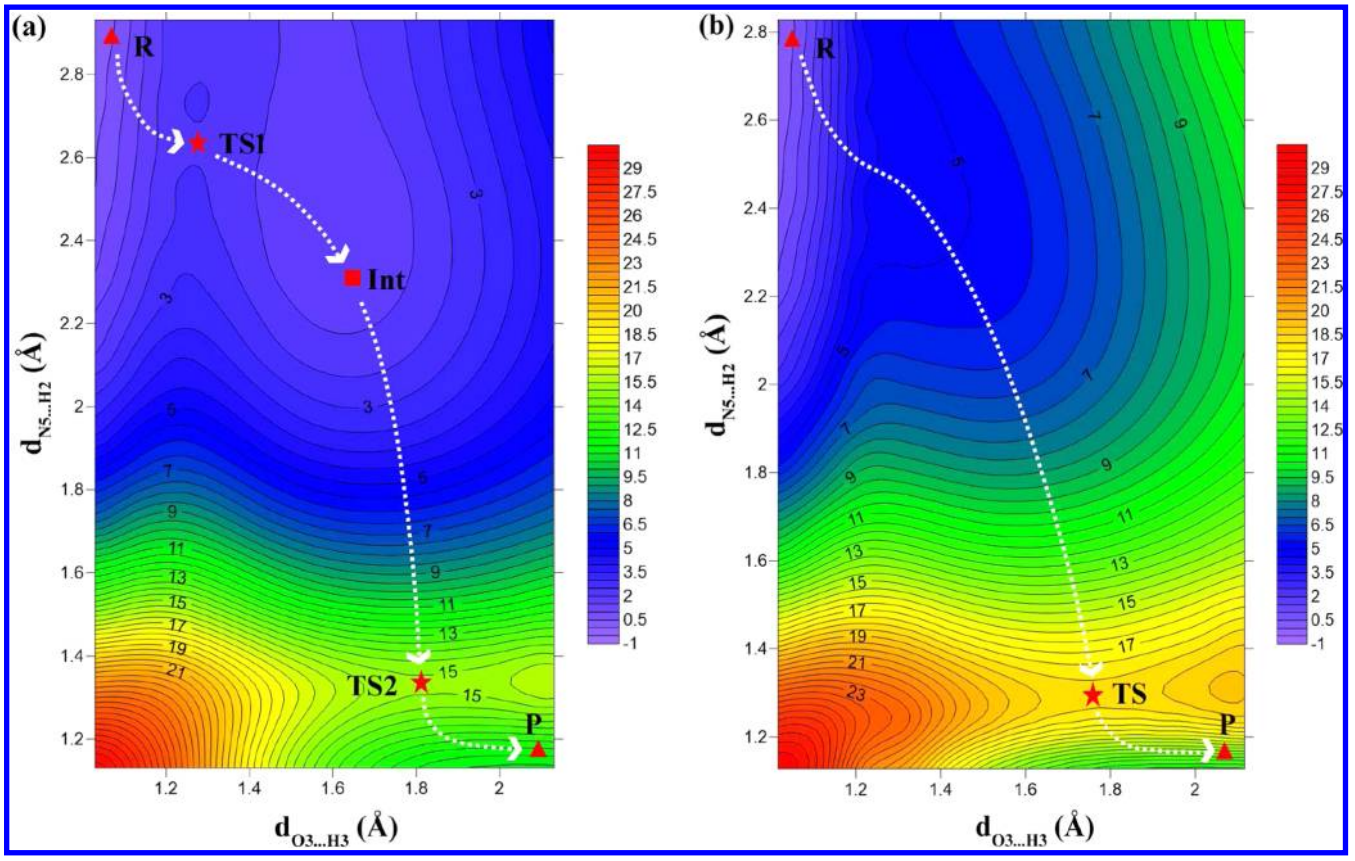

Figure 6. 2D-PES scan of HT mechanism of (a) WT system and (b) Y129F mutant system at the ONIOM-ME (B3LYP/6-31G(d,p):AMBER) level.

Phe129 contribute −0.69 and −0.26 kcal/mol, respectively, to L-lactate's binding to LCHAO and its mutant Y129F. The less contribution of Phe129 in mutant could be attributed to the missing hydrogen bond between the residue Phe129 and L-lactate. However, this unfavorable effect for the Y129F mutant LCHAO was estimated to be counteracted by other residues. It was observed in the MD trajectories that the carboxyl group of L-lactate drifted slightly in the mutant but was more stable in WT during the simulations, making the negative center of L-lactate move a little away from Arg164, His247, Arg250, and FMN but stay closer to K201 in the Y129F mutant than in WT LCHAO. The overall contributions of these residues were more negative in the mutant (−25.00 kcal/mol) than in the WT (−22.83 kcal/mol), thus counteracting the loss of the hydrogen bond in the mutant and resulting in similar binding free energy in total.

QM/MM Calculations of HT Mechanism of L-Lactate's Dehydrogenation Promoted by LCHAO. In order to get a better understanding of the HT mechanism, we thoroughly explored the QM/MM potential energy surface (PES) of the reaction using distinguished reaction coordinates prior to the final optimization of the stationary points. In the proposed HT mechanism, the proton in the α-OH group of L-lactate is first transferred to the imidazole group of the residue His247 and α-H is then transferred to the isoalloxazinyl ring of FMN as a hydride in the second step. As illustrated in Figure 6a for the PES calculations, we scanned the distance $d_{O3\cdots H3}$, which characterizes the proton-transfer process, between the atoms O3 and H3 of L-lactate and the distance $d_{N5\cdots H2}$, which determines the formation of the new N5−H2 linkage, between the N5 atom of FMN and the H2 atom of L-lactate. Each calculated point on the PES corresponds to the optimized structure for the given distances $d_{O3\cdots H3}$ and $d_{N5\cdots H2}$ at ONIOM (B3LYP/6-31G(d,p):AMBER) level with the mechanical embedding (ME) scheme implemented. From the two-dimensional (2D) reaction coordinate contour map (Figure 6a), it can be clearly identified that there are one intermediate (Int) and two transition states TS1 and TS2. Therefore, the 2D-PES energy profile indicated that the HT reaction would proceed through a stepwise mechanism from the reactant (R) to the product (P) with two distinct steps of the His-catalyzed deprotonation of α-OH and the hydride transfer from substrate to FMN. According to the 2D-PES scanning, the reaction barriers could be about 2.5 kcal/mol for the first step and about 13.5 kcal/mol for the second step, revealing that the transfer of the α-H as a hydride to the N5 atom of FMN is a rate-limiting step in the whole catalytic process.

To obtain the exact structure of each stationary point along reaction pathway and study the reaction barrier more accurately, further QM/MM calculations were conducted on the basis of the predicted intermediate and two transition states pointed in the 2D-PES map. As displayed in Figure S3a−e in the Supporting Information, the optimized structures of reactant, TS1, intermediate, TS2, and product were finally obtained at the level of ONIOM-EE (B3LYP/6-31G-(d,p):AMBER). As listed in Table S1 in the Supporting Information, reaction barriers were calculated to be 6.1 and 10.5 kcal/mol, respectively, for the first and second steps at the level of ONIOM-EE (B3LYP/6-31G(d,p):AMBER). As compared to the 2D-PES results using ONIOM-ME method, the barrier height was estimated to be higher (6.1 versus 2.5 kcal/mol) for the first step while lower for the second (10.5

dx.doi.org/10.1021/jp5022399 | J. Phys. Chem. B 2014, 118, 5406−5417

versus 13.5 kcal/mol) when incorporating the partial charges of the MM region into the quantum mechanical Hamiltonian. This result indicated that the electrostatic potential of the MM region would be unfavorable to the proton abstraction by His247 in the first step but advantageous to hydride transferring to FMN in the second step. To understand the reaction barriers more accurately, each ONIOM-EE optimized stationary point was then submitted to single-point energy calculations at ONIOM-EE (B3LYP/6-311++G(d,p):AMBER), ONIOM-EE (ωB97X/6-311++G(d,p):AMBER), and ONIOM-EE (ωB97XD/6-311++G(d,p):AMBER) level of theory. The results are listed in Table 2 as ΔE for the change

Table 2. Reaction Energy Profile of LCHAO-FMN-Lactate(HT) and LCHAO(Y129F)-FMN-Lactate(HT) Following HT Mechanism (kcal/mol)

	B3LYP[a]		ωB97X[b]		ωB97XD[c]	
	ΔE	ΔG	ΔE	ΔG	ΔE	ΔG
	LCHAO-FMN-Lactate(HT)					
R	0.0	0.0	0.0	0.0	0.0	0.0
TS1	7.9	6.5	7.7	6.4	6.4	5.0
Int	7.7	6.3	7.6	6.1	6.3	4.8
TS2	17.2	14.6	22.7	20.0	18.3	15.7
P	−2.6	−3.9	−4.2	−5.5	−5.1	−6.3
	LCHAO(Y129F)-FMN-lactate(HT)					
R	0.0	0.0	0.0	0.0	0.0	0.0
TS	19.9	16.4	26.0	22.5	21.3	17.9
P	−2.8	−4.6	−4.9	−6.6	−5.4	−7.2

[a]Relative (to reactant) total electronic energy (ΔE) and Gibbs Free energy (ΔG, with thermal correction) at B3LYP/6-311++G-(d,p):AMBER//B3LYP/6-31G(d,p):AMBER level. [b]Relative (to reactant) total electronic energy (ΔE) and Gibbs free energy (ΔG, with thermal correction) at ωb97X/6-311++G(d,p):AMBER//B3LYP/6-31G(d,p):AMBER level. [c]Relative (to reactant) total electronic energy (ΔE) and Gibbs Free energy (ΔG, with thermal correction) at ωb97XD/6-311++G(d,p):AMBER//B3LYP/6-31G-(d,p):AMBER level.

of potential energy along the reaction progress. Gibbs free energies were then obtained on the basis of calculated potential energies and thermal correction following the method described in the Computational Details. As shown in Table 2, the barrier heights of Gibbs free energy (ΔG) using B3LYP, ωB97X, and ωB97XD methods were calculated to be 6.5, 6.4, and 5.0 kcal/mol, respectively, for the first step and 8.3, 13.9, and 10.8 kcal/mol, respectively, for the second step. Our results showed that the ΔG is smaller than the corresponding ΔE, indicating that the enzymatic environment and thermodynamical effects are to the benefit of the reaction. Taken together, the second step regarding the hydride transfer from L-lactate to FMN is a rate-limiting step while the barrier is also not negligible for the deprotonation of α-OH of the substrate. According to our calculations using higher level and different methods, energies of TS1 and Int are close, indicating a flat energy surface during the transformation from TS1 to Int. That is in accordance with our 2D-PES scan results, which could be attributed to the low pK_a (approximately 6.0)[57] of the side-chain imidazole group of His247. The doubly protonated state of His247 with relatively high energy would have salt bridge interaction with the side-chain carboxyl group of Asp157. According to Table 2, in contrast to the endothermic process of step one, step two is exothermic, releasing 10.2 kcal/mol (B3LYP), 11.6 kcal/mol (ωB97X), or 11.1 kcal/mol (ωB97XD), which is to the benefit of hydride transfer from L-lactate to FMN.

QM/MM Calculations of HT Mechanism of Y129F Mutant LCHAO. On the basis of MD-simulated structural model of complex LCHAO(Y129F)-FMN-lactate(HT), we further performed the QM/MM calculations to investigate the effects of the key residue Tyr129 on the LCHAO-catalyzed oxidation reaction of L-lactate. As discussed above, our MD simulations indicated that phenolic hydroxyl group of Tyr129 may form an H-bonding interaction, which would be dismissed in Y129F mutant LCHAO, with the α-hydroxyl group of the substrate L-lactate. Such a dismissed H-bond would not influence the calculated binding free energies of L-lactate, which is congruent with the biochemical data.[38,39] On the other hand, the QM/MM computations on the system LCHAO-(Y129F)-FMN-lactate(HT) would theoretically demonstrate whether the missing H-bond changes the mechanism of the LCHAO(Y129F) catalyzed oxidation reaction. Similar to the QM/MM calculations on LCHAO-FMN-lactate(HT), the PES calculations were also performed by scanning the distances $d_{O3\cdots H3}$ and $d_{N5\cdots H2}$, respectively. As shown in Figure 6b for the obtained PES maps, only one transition state observed from the 2D-PES scan testified that processes of the OH bond cleavage and NH bond formation would be concerted. Therefore, the Y129F mutant LCHAO would catalyze the oxidation of L-lactate in one step, which is different from a stepwise process as happened in WT LCHAO catalyzed oxidation. Actually, primary and solvent kinetic isotope studies, reported by Sobrado et al.,[26] on both WT and Y254F mutant FCB2 concluded that the L-lactate CH and OH bond cleavages were stepwise in WT FCB2 enzyme while concerted in its Y254F mutant. Because of the high conservation of the reaction center among the enzyme family, LCHAO may be hypothesized to follow the same regulation as FCB2. Furthermore, the hydrogen/deuterium kinetic isotope effects (KIEs) on the α-H of L-lactate were calculated from the frequency analyses for both WT and Y129F mutant LCHAO systems using the program ISOEFF98.[58] The results are 4.6 for WT and 5.0 for Y129F mutant LCHAO, which are consistent with the experimental values for FCB2 (4.5 ± 1.1 for WT and 5.4 ± 0.4 for Y254F mutant).[38] Although the experimental KIEs for LCHAO are unavailable, these data somehow validate the rationality of HT mechanism.

As illustrated in Figure S3f–h in the Supporting Information, full-optimization QM/MM calculations were performed to obtain the reactant, transition state, and product state of LCHAO(Y129F)-FMN-lactate(HT) at the B3LYP/6-311++G-(d,p):AMBER//B3LYP/6-31G(d,p):AMBER level on the basis of PES calculations. Based on the reported biochemical data[38,39] about k_{cat} values of WT FCB2 ($k_{cat}^{WT\ FCB2}$ = 6.10 ± 0.25 s^{-1}) and Y254F mutant FCB2 ($k_{cat}^{Y254\ mutant\ FCB2}$ = 270 ± 30 s^{-1}) and WT GOX ($k_{cat}^{WT\ GOX}$ = 25 s^{-1}) and Y129F mutant GOX ($k_{cat}^{Y129F\ mutant\ GOX}$ = 0.63 s^{-1}), the reaction barrier would increase by approximately 2.3 kcal/mol according to eq 1[29]

$$\Delta G^{mutant} - \Delta G^{WT} = -RT \ln[k_{cat}^{mutant}/k_{cat}^{WT}] \quad (1)$$

when high-conserved Tyr in the active site is mutated to Phe for FMN-dependent L-α-hydroxy acid oxidases. As shown in Figure 7, the barrier height (Gibbs free energy) of the HT mechanism is 16.4 kcal/mol of Y129F mutant LCHAO while about 14.8 kcal/mol (the sum of the two steps) of WT LCHAO, which is 1.6 kcal/mol lower than the mutant,

dx.doi.org/10.1021/jp5022399 | J. Phys. Chem. B 2014, 118, 5406−5417

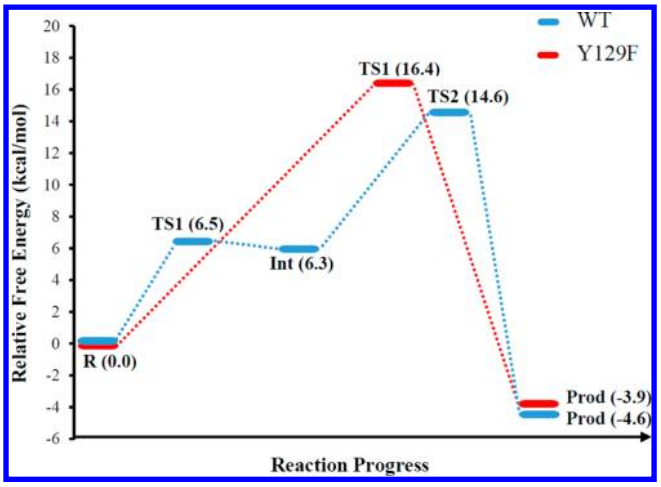

Figure 7. Reaction free energy profiles of L-lactate catalyzed by WT (blue) and Y129F mutant (red) LCHAO following HT mechanism. Energies were obtained at the B3LYP/6-311++G(d,p):AMBER//B3LYP/6-31G(d,p):AMBER level with thermal correction to Gibbs free energy.

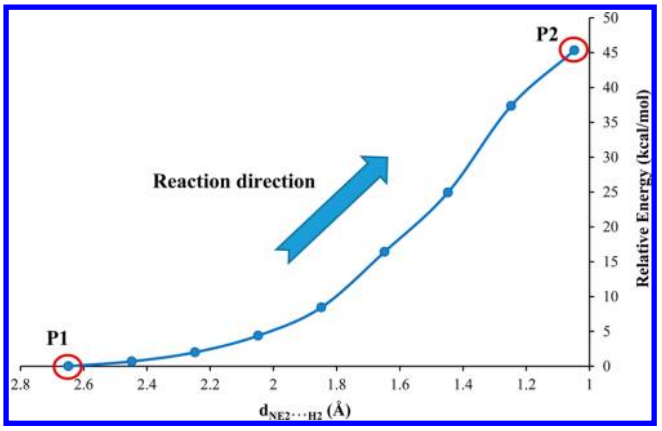

Figure 8. Energy scan of CA mechanism at the ONIOM-EE (B3LYP/6-31G(d,p):AMBER) level. The arrow shows the $d_{NE2\cdots H2}$ variation along the process of α-H transfer to the NE2 atom of His247. P1 is the reactant in which $d_{NE2\cdots H2}$ = 2.65 Å. P2 represents for the proposed "product" with $d_{NE2\cdots H2}$ = 1.05 Å. Energy scan was conducted from P1 to P2 in steps of 0.2 Å with each point optimized.

according to our energy profile obtained at the B3LYP/6-311++G(d,p):AMBER//B3LYP/6-31G(d,p):AMBER level. In addition, both ωB97X and ωB97XD computed total barriers of LCHAO are about 2 kcal/mol lower than its mutant (Table 2). Our theoretically calculated data are congruent with the experimental data very well. Therefore, the high conserved residue tyrosine (Tyr129 in LCHAO) plays critical role in the kinetic rate of L-α-hydroxy acid's dehydrogenation catalyzed by FMN-dependent L-α-hydroxy acid oxidases by forming an H-bond interaction with L-α-hydroxy group of substrate. In the meantime, these calculation results verify again the proposed HT mechanism.

QM/MM Calculations of CA Mechanism of LCHAO. As discussed above, MD simulations indicated that it would be not stable for L-lactate to bind to LCHAO in a mode for its dehydrogenation with a proposed CA mechanism. However, our further ab initio computations at the level of B3LYP/6-311++G(d,p) indicated that L-lactate has corresponding energy about 7 kcal/mol for reciprocal transformation from Φ(O3−C2−C1−O1) = 0° to Φ(O3−C2−C1−O1) = 180° (Figure S4 in the Supporting Information), which means the single bond C1−C2 would rotate flexibly. Therefore, QM/MM calculations were also performed to validate the possibility of an assumed CA mechanism. As indicated above, the carbanoin mechanism would be started with the formation of a carbanoin by the substrate's α-proton transferring to the imidazole side chain of the residue His247 (in LCHAO). However, the whereabouts of the proton of α-OH as well as the mechnism of transfer of two electrons from the carbanion to the flavin are still unclear. In view of these, in our present QM/MM calculaitons, we only probed into the generally accepted abstraction of α-H regarding the CA mechanism. To examine the energy profile of the formation of carbanion, the distance $d_{NE2\cdots H2}$ was scanned at the ONIOM-EE (B3LYP/6-31G(d,p):AMBER) level to study the PES of proton transfer from α-C of L-lactate to NE2 atom of His247. In the energy scan, each point was optimized with given NE2−H2 bond distance. As shown in Figure 8, the system suffered a sustained energy rise during the whole process. From the reactant to the last scanned point, the energy increased nearly 45 kcal/mol, which is much higher than those calculated in the HT mechanism, and no transition state was found for the proposed carbanoin mechanism. These results may clearify that the formation of carbanion would be energetically disfavorable.

CONCLUSIONS

In the present work, the two proposed mechanisms of flavin-reductive half-reaction in the oxidation of L-α-hydroxy acid by LCHAO were compared using MD simulations and QM/MM method. The conformation of L-lactate remained stable during the last 20 ns MD simulations in the case of HT binding mode, while L-lactate inclined to change its conformation to suit hydride transfer when initially binding in the CA mode, indicating that the HT mechanism is thermodynamically more favorable. Moreover, according to the PES scan using QM/MM method, the energy barrier of carbanion formation is too high to overcome while the oxidation of L-lactate could successfully proceed through a two-step HT reaction. In addition, our MD and QM/MM calculations further demonstrated that the highly conserved residue Tyr129 in the active site plays a critical role to the process of LCHAO-catalyzed dehydrogenation of L-lactate by in silico mutation of Tyr129 to Phe. In summary, both the results of MD simulations and QM/MM calculations congruously support the HT mechanism. This computational work gave a better understanding of LCHAO's catalysis characteristics toward L-lactate in the flavin-reductive half-reaction. Although only L-lactate was studied here, other substrates such as L-mandelate and L-α-hydroxy octanoate could also follow the same HT mechanism in the oxidation process by LCHAO. More importantly, in consideration of the high conservation of the catalytic center among the FMN-dependent L-α-hydroxy acid oxidase enzyme family, our studies may provide a valuable reference for the catalytic mechanism of other enzymes including FCB2, MDH, GOX, HAOX1, HAOX2, and HAOX3.

ASSOCIATED CONTENT

Supporting Information

Superposition of crystal structures of FMN-dependent L-α-hydroxy acid oxidases, sequence alignments of FMN-dependent L-α-hydroxy acid oxidases (LCHAO, FCB2, MDH, GOX, HAOX1, HAOX2, HAOX3), the QM/MM-optimized struc-

dx.doi.org/10.1021/jp5022399 | J. Phys. Chem. B 2014, 118, 5406−5417

tures of reactants, transition states, and products at the level of ONIOM-EE (B3LYP/6-31G(d,p):AMBER), computations of rotation energy barrier of L-lactate for reciprocal transformation from Φ(O3−C2−C1−O1) = 0° to Φ(O3−C2−C1−O1) = 180°. This material is available free of charge via the Internet at http://pubs.acs.org.

AUTHOR INFORMATION

Corresponding Author

*Tel.: 86-571-88208659. E-mail: chjz@zju.edu.cn.

Notes

The authors declare no competing financial interest.

ACKNOWLEDGMENTS

This work was supported by National Science Foundation of China (grant NO. 81172983). We also thank Prof. Piotr Paneth, from the Institute of Applied Radiation Chemistry, Lodz University of Technology, Lodz, Poland, to provide us the software ISOEFF.

ABBREVIATIONS

LCHAO, long-chain L-α-hydroxy acid oxidase; CA, carbanion; HT, hydride transfer; WT, wild-type; FMN, flavin mononucleotide; MD, molecular dynamics; QM/MM, quantum mechanics/molecular mechanics; FCB2, yeast flavocytochrome b_2; MDH, mandelate dehydrogenase from *Pseudomonas putida*; GOX, spinach glycolate oxidase; hGOX, human glycolate oxidase; HAOX2, human L-α-hydroxy acid oxidase 2; HAOX3, human L-α-hydroxy acid oxidase 3; CCPST, 4-carboxy-5-[(4-chlorophenyl)sulfanyl]-1,2,3-thiadiazole; R, reactant; TS, transition state; Int, intermediate; P, product; PES, potential energy surface; ME, mechanical embedding; EE, electronic embedding

REFERENCES

(1) Blanchard, M.; Green, D.; Nocito, V.; Ratner, S. L-Amino Acid Oxidase of Animal Tissue. *J. Biol. Chem.* **1944**, *155*, 421−440.

(2) Blanchard, M.; Green, D.; Nocito-Carroll, V.; Ratner, S. L-Hydroxy Acid Oxidase. *J. Biol. Chem.* **1946**, *163*, 137−144.

(3) Belmouden, A.; Lederer, F. The Role of a β Barrel Loop 4 Extension in Modulating the Physical and Functional Properties of Long-Chain 2-Hydroxy-Acid Oxidase Isozymes. *Eur. J. Biochem.* **1996**, *238*, 790−798.

(4) Ozasa, H.; Horikawa, S.; Ota, K. Methylguanidine Synthase from Rat Kidney Is Identical to Long-Chain L-2-Hydroxy Acid Oxidase. *Nephron* **1994**, *68*, 279−279.

(5) Yokozawa, T.; Fujitsuka, N.; Oura, H.; Akao, T.; Kobashi, K.; Ienaga, K.; Nakamura, K.; Hattori, M. Purification of Methylguanidine Synthase from the Rat Kidney. *Nephron* **1993**, *63*, 452−457.

(6) De Deyn, P.; Marescau, B.; Lornoy, W.; Becaus, I.; Van Leuven, I.; Van Gorp, L.; Lowenthal, A. Serum Guanidino Compound Levels and the Influence of a Single Hemodialysis in Uremic Patients Undergoing Maintenance Hemodialysis. *Nephron* **1987**, *45*, 291−295.

(7) De Deyn, P. P.; D'hooge, R.; Van Bogaert, P.-P.; Marescau, B. Endogenous Guanidino Compounds as Uremic Neurotoxins. *Kidney Int.* **2001**, *59*, S77−S83.

(8) Chen, Z.-w.; Vignaud, C.; Jaafar, A.; Lévy, B.; Guéritte, F.; Guénard, D.; Lederer, F.; Mathews, F. S. High Resolution Crystal Structure of Rat Long Chain Hydroxy Acid Oxidase in Complex with the Inhibitor 4-Carboxy-5-[(4-Chlorophenyl) Sulfanyl]-1, 2, 3-Thiadiazole. Implications for Inhibitor Specificity and Drug Design. *Biochimie* **2012**, *94*, 1172−1179.

(9) Muller, F. *Chemistry and Biochemistry of Flavoenzymes*; CRC Press: Boca Raton, FL, 1991.

(10) Lehoux, I. E.; Mitra, B. (S)-Mandelate Dehydrogenase from *Pseudomonas Putida*: Mechanistic Studies with Alternate Substrates and pH and Kinetic Isotope Effects. *Biochemistry* **1999**, *38*, 5836−5848.

(11) Lindqvist, Y. Refined Structure of Spinach Glycolate Oxidase at 2 Å Resolution. *J. Mol. Biol.* **1989**, *209*, 151−166.

(12) Murray, M. S.; Holmes, R. P.; Lowther, W. T. Active Site and Loop 4 Movements within Human Glycolate Oxidase: Implications for Substrate Specificity and Drug Design. *Biochemistry* **2008**, *47*, 2439−2449.

(13) Jones, J. M.; Morrell, J. C.; Gould, S. J. Identification and Characterization of HAOX1, HAOX2, and HAOX3, Three Human Peroxisomal 2-Hydroxy Acid Oxidases. *J. Biol. Chem.* **2000**, *275*, 12590−12597.

(14) Cunane, L. M.; Barton, J. D.; Chen, Z.-w.; Lê, K. D.; Amar, D.; Lederer, F.; Mathews, F. S. Crystal Structure Analysis of Recombinant Rat Kidney Long Chain Hydroxy Acid Oxidase. *Biochemistry* **2005**, *44*, 1521−1531.

(15) Ghisla, S.; Massey, V. Mechanisms of Flavoprotein-Catalyzed Reactions. *Eur. J. Biochem.* **1989**, *181*, 1−17.

(16) Lindqvist, Y.; Brändén, C.; Mathews, F. S.; Lederer, F. Spinach Glycolate Oxidase and Yeast Flavocytochrome b_2 Are Structurally Homologous and Evolutionarily Related Enzymes with Distinctly Different Function and Flavin Mononucleotide Binding. *J. Biol. Chem.* **1991**, *266*, 3198−3207.

(17) Maeda-Yorita, K.; Aki, K.; Sagai, H.; Misaki, H.; Massey, V. L-Lactate Oxidase and L-Lactate Monooxygenase: Mechanistic Variations on a Common Structural Theme. *Biochimie* **1995**, *77*, 631−642.

(18) Stenberg, K.; Clausen, T.; Lindqvist, Y.; Macheroux, P. Involvement of Tyr24 and Trp108 in Substrate Binding and Substrate Specificity of Glycolate Oxidase. *Eur. J. Biochem.* **1995**, *228*, 408−416.

(19) Mowat, C. G.; Wehenkel, A.; Green, A. J.; Walkinshaw, M. D.; Reid, G. A.; Chapman, S. K. Altered Substrate Specificity in Flavocytochrome b2: Structural Insights into the Mechanism of L-lactate Dehydrogenation. *Biochemistry* **2004**, *43*, 9519−9526.

(20) Dijkman, W. P.; de Gonzalo, G.; Mattevi, A.; Fraaije, M. W. Flavoprotein Oxidases: Classification and Applications. *Appl. Microbiol. Biotechnol.* **2013**, *97*, 5177−5188.

(21) Walsh, C. T.; Wencewicz, T. A. Flavoenzymes: Versatile Catalysts in Biosynthetic Pathways. *Nat. Prod. Rep.* **2013**, *30*, 175−200.

(22) Ghisla, S.; Massey, V. Studies on the Mechanism of Action of the Flavoenzyme Lactate Oxidase. *J. Biol. Chem.* **1977**, *252*, 6729−6735.

(23) Rao, K. S.; Lederer, F. About the pKa of the Active-Site Histidine in Flavocytochrome b_2 (Yeast L-Lactate Dehydrogenase). *Protein Sci.* **1998**, *7*, 1531−1537.

(24) Dewanti, A. R.; Mitra, B. A Transient Intermediate in the Reaction Catalyzed by (S)-Mandelate Dehydrogenase from *Pseudomonas Putida*. *Biochemistry* **2003**, *42*, 12893−12901.

(25) Fitzpatrick, P. F. Carbanion versus Hydride Transfer Mechanisms in Flavoprotein-Catalyzed Dehydrogenations. *Bioorg. Chem.* **2004**, *32*, 125−139.

(26) Sobrado, P.; Fitzpatrick, P. F. Solvent and Primary Deuterium Isotope Effects Show that Lactate CH and OH Bond Cleavages are Concerted in Y254F Flavocytochrome b_2, Consistent with a Hydride Transfer Mechanism. *Biochemistry* **2003**, *42*, 15208−15214.

(27) Sinclair, R.; Reid, G.; Chapman, S. Re-Design of Saccharomyces Cerevisiae Flavocytochrome b_2: Introduction of L-Mandelate Dehydrogenase Activity. *Biochem. J.* **1998**, *333*, 117−120.

(28) Daff, S.; Manson, F.; Reid, G.; Chapman, S. K. Strategic Manipulation of the Substrate Specificity of Saccharomyces Cerevisiae Flavocytochrome b_2. *Biochem. J.* **1994**, *301*, 829−834.

(29) Gondry, M.; Dubois, J.; Terrier, M.; Lederer, F. The Catalytic Role of Tyrosine 254 in Flavocytochrome b2 (L-Lactate Dehydrogenase from Baker's Yeast). *Eur. J. Biochem.* **2001**, *268*, 4918−4927.

(30) Liao, R.-Z.; Thiel, W. Comparison of QM-Only and QM/MM Models for the Mechanism of Tungsten-Dependent Acetylene Hydratase. *J. Chem. Theory Comput.* **2012**, *8*, 3793−3803.

(31) van der Kamp, M. W.; Mulholland, A. J. Combined Quantum Mechanics/Molecular Mechanics (QM/MM) Methods in Computational Enzymology. *Biochemistry* **2013**, *52*, 2708−2728.

(32) Wang, Z.; Ferrer, S.; Moliner, V.; Kohen, A. QM/MM Calculations Suggest a Novel Intermediate Following the Proton Abstraction Catalyzed by Thymidylate Synthase. *Biochemistry* **2013**, *52*, 2348−2358.
(33) Kim, Y.; Zhou, M.; Moy, S.; Morales, J.; Cunningham, M. A.; Joachimiak, A. High-Resolution Structure of the Nitrile Reductase QueF Combined with Molecular Simulations Provide Insight into Enzyme Mechanism. *J. Mol. Biol.* **2010**, *404*, 127−137.
(34) Cheng, Y.; Zhang, F.; Chen, Q.; Gao, J.; Cui, W.; Ji, M.; Tung, C.-H. Structural Basis of Specific Binding Between Aurora A and TPX2 by Molecular Dynamics Simulations. *J. Chem. Inf. Model.* **2011**, *51*, 2626−2635.
(35) Yang, Y.; Qin, J.; Liu, H.; Yao, X. Molecular Dynamics Simulation, Free Energy Calculation and Structure-Based 3D-QSAR Studies of B-RAF Kinase Inhibitors. *J. Chem. Inf. Model.* **2011**, *51*, 680−692.
(36) Pan, P.; Li, Y.; Yu, H.; Sun, H.; Hou, T. Molecular Principle of Topotecan Resistance by Topoisomerase I Mutations through Molecular Modeling Approaches. *J. Chem. Inf. Model.* **2013**, *53*, 997−1006.
(37) Angkawidjaja, C.; Matsumura, H.; Koga, Y.; Takano, K.; Kanaya, S. X-ray Crystallographic and MD Simulation Studies on the Mechanism of Interfacial Activation of a Family I. 3 Lipase with Two Lids. *J. Mol. Biol.* **2010**, *400*, 82−95.
(38) Dubois, J.; Chapman, S. K.; Mathews, F. S.; Reid, G. A.; Lederer, F. Substitution of Tyr254 with Phe at the Active Site of Flavocytochrome b_2: Consequences on Catalysis of Lactate Dehydrogenation. *Biochemistry* **1990**, *29*, 6393−6400.
(39) Macheroux, P.; Kieweg, V.; Massey, V.; Söderlind, E.; Stenberg, K.; Lindqvist, Y. Role of Tyrosine 129 in the Active Site of Spinach Glycolate Oxidase. *Eur. J. Biochem.* **1993**, *213*, 1047−1054.
(40) Fiser, A.; Sali, A. ModLoop: Automated Modeling of Loops in Protein Structures. *Bioinformatics* **2003**, *19*, 2500−2501.
(41) Langkilde, A.; Oddershede, J.; Larsen, S. Diastereomeric Salts of Lactic Acid and 1-Phenylethylamine, Their Structures and Relative Stabilities. *Acta Crystallogr. Sect. B: Struct. Sci.* **2002**, *58*, 1044−1050.
(42) Case, D.; Darden, T.; Cheatham III, T.; Simmerling, C.; Wang, J.; Duke, R.; Luo, R.; Walker, R.; Zhang, W.; Merz, K.; et al. *AMBER 12*; University of California: San Francisco, CA, 2012.
(43) Li, H.; Robertson, A. D.; Jensen, J. H. Very Fast Empirical Prediction and Rationalization of Protein pKa Values. *Proteins: Struct., Funct., Bioinf.* **2005**, *61*, 704−721.
(44) Case, D. A.; Cheatham, T. E.; Darden, T.; Gohlke, H.; Luo, R.; Merz, K. M.; Onufriev, A.; Simmerling, C.; Wang, B.; Woods, R. J. The Amber Biomolecular Simulation Programs. *J. Comput. Chem.* **2005**, *26*, 1668−1688.
(45) Frisch, M. E.; Trucks, G.; Schlegel, H. B.; Scuseria, G.; Robb, M.; Cheeseman, J.; Scalmani, G.; Barone, V.; Mennucci, B.; Petersson, G. E.; et al. *Gaussian 09, revision C.1*; Gaussian, Inc.: Wallingford, CT, 2009.
(46) Schneider, C.; Sühnel, J. A Molecular Dynamics Simulation of the Flavin Mononucleotide−RNA Aptamer Complex. *Biopolymers* **1999**, *50*, 287−302.
(47) Darden, T.; York, D.; Pedersen, L. Particle Mesh Ewald: An *N*·log (*N*) Method for Ewald Sums in Large Systems. *J. Chem. Phys.* **1993**, *98*, 10089.
(48) Ryckaert, J.-P.; Ciccotti, G.; Berendsen, H. J. Numerical Integration of the Cartesian Equations of Motion of a System with Constraints: Molecular Dynamics of *n*-Alkanes. *J. Comput. Phys.* **1977**, *23*, 327−341.
(49) Gohlke, H.; Kiel, C.; Case, D. A. Insights into Protein−Protein Binding by Binding Free Energy Calculation and Free Energy Decomposition for the Ras-Raf and Ras-RalGDS Complexes. *J. Mol. Biol.* **2003**, *330*, 891−913.
(50) Chen, S.-F.; Cao, Y.; Chen, J.-J.; Chen, J.-Z. Binding Selectivity Studies of PKBα Using Molecular Dynamics Simulation and Free Energy Calculations. *J. Mol. Model.* **2013**, *19*, 5097−5112.
(51) Tian, B.-X.; Eriksson, L. A. Catalytic Mechanism and Product Specificity of Oxidosqualene-Lanosterol Cyclase: A QM/MM Study. *J. Phys. Chem. B* **2012**, *116*, 13857−13862.
(52) Cerón-Carrasco, J. P.; Jacquemin, D.; Graton, J. r. m.; Thany, S.; Le Questel, J.-Y. New Insights on the Molecular Recognition of Imidacloprid with Aplysia Californica AChBP: A Computational Study. *J. Phys. Chem. B* **2013**, *117*, 3944−3953.
(53) Lundberg, M.; Sasakura, Y.; Zheng, G.; Morokuma, K. Case Studies of ONIOM (DFT: DFTB) and ONIOM (DFT: DFTB: MM) for Enzymes and Enzyme Mimics. *J. Chem. Theory Comput.* **2010**, *6*, 1413−1427.
(54) Bakowies, D.; Thiel, W. Hybrid Models for Combined Quantum Mechanical and Molecular Mechanical Approaches. *J. Phys. Chem.* **1996**, *100*, 10580−10594.
(55) Sukumar, N.; Dewanti, A.; Merli, A.; Rossi, G. L.; Mitra, B.; Mathews, F. S. Structures of the G81A Mutant Form of the Active Chimera of (S)-mandelate Dehydrogenase and Its Complex with Two of Its Substrates. *Acta Crystallogr. Sect. D. Biol. Crystallogr.* **2009**, *65*, 543−552.
(56) Lightstone, F. C.; Bruice, T. C. Ground State Conformations and Entropic and Enthalpic Factors in the Efficiency of Intramolecular and Enzymatic Reactions. 1. Cyclic Anhydride Formation by Substituted Glutarates, Succinate, and 3, 6-Endoxo-Δ^4-Tetrahydrophthalate Monophenyl Esters. *J. Am. Chem. Soc.* **1996**, *118*, 2595−2605.
(57) Tanokura, M. ^{1}H-NMR Study on the Tautomerism of the Imidazole Ring of Histidine Residues: I. Microscopic pK Values and Molar Ratios of Tautomers in Histidine-Containing Peptides. *Biochim. Biophys. Acta* **1983**, *742*, 576−585.
(58) Anisimov, V.; Paneth, P. ISOEFF98. A Program for Studies of Isotope Effects Using Hessian Modifications. *J. Math. Chem.* **1999**, *26*, 75−86.
(59) Nguyen, D. T.; Case, D. A. On Finding Stationary States on Large-Molecule Potential Energy Surfaces. *J. Phys. Chem.* **1985**, *89*, 4020−4026.